TÜBİTAK

Turkish Journal of Chemistry

http://journals.tubitak.gov.tr/chem/

Research Article

Turk J Chem
(2014) 38: 1046 – 1055

doi:10.3906/kim-1406-39

Nature of second-order nonlinear optical response in phthalocyanine derivatives: a density functional theory study

Chiming WANG, Chao CHEN, Qingqi ZHANG, Dongdong QI*, Jianzhuang JIANG

Beijing Key Laboratory for Science and Application of Functional Molecular and Crystalline Materials, Department of Chemistry, University of Science and Technology Beijing, Beijing, P.R. China

Received: 15.06.2014 • **Accepted:** 07.08.2014 • **Published Online:** 24.11.2014 • **Printed:** 22.12.2014

Abstract: Density functional theory was employed to investigate a series of phthalocyanine derivatives, discovering the limitation when the expansion of the conjugated system was employed to improve the hyper-Rayleigh scattering response coefficient. Furthermore, an unusually $C_{\infty v}$-type octupolar population was found by electrostatic potential analysis. In addition, the dynamic and static hyper-Rayleigh scattering responses (β_{HRS}) were simulated using the coupled perturbed density functional theory, showing an increasing dynamic β_{HRS} value along with an increase in incident light energy.

Key words: Phthalocyanine, DFT, second-order NLO, dipolar moment, octupolar moment

1. Introduction

Nonlinear optical (NLO) materials have been intensively studied in recent decades because of their extensive applications in the fields of all-optical switching, optical information storage, laser frequency conversion devices, ultrafast modulators, and optical sensors.[1–5] However, traditional inorganic materials still have some obvious drawbacks, such as low response coefficient, long response time, normal laser-damaged threshold, and difficulty in substitution.[6] Fortunately, these limitations can be easily overcome when employing organic dipolar/octupolar molecules, leading to a new family of organic NLO materials.[7]

Essentially, the nonlinear optical effect is caused by the periodic vibration of the intramolecular electronic field driven by the external electromagnetic field.[8] A high-performance second-order nonlinear optical molecular material must possesses 2 factors, adequate free π electrons and a broad oscillating space.[9] Phthalocyanines (Pcs) were widely studied in the past century because of their special macrocyclic electron-delocalizing structures, which just meet these 2 factors.[10] In addition, the ease of peripheral substitution renders the phthalocyanine ring a representative skeleton to investigate the relationship between the second-order nonlinear optical effect and electron-donating/-withdrawing substituents.[11]

In the present study, density functional theory (DFT),[12] time-dependent density functional theory (TD-DFT),[13] and coupled perturbed density functional theory (CP-DFT)[14,15] were used to investigate the linear and nonlinear optical properties of Pc/Por and their derivatives. The ratio of dipolar/octupolar contribution, the harmonic light intensity as a function of the polarization angle by polar representation, and the intramolecular electronic density oscillation driven by the external electromagnetic field were also calculated in order to clarify the nonlinear optical nature of functional Pc molecular materials.

*Correspondence: qdd@ustb.edu.cn

2. Results and discussion

In the present paper, a series of Pc derivatives are indicated in Scheme 1. According to the electronegativity order, the peripheral substituents are selected from –CH=CH_2/–PH_2 of –0.05/+0.04, –CH_3/–Cl of –0.17/+0.23, –$NHNH_2$/–$COCH_3$ of –0.55/+0.50, to –NHMe/-ONO_2 of –0.70/+0.70.[16] Each molecule is named B_nR_n (Scheme 1).

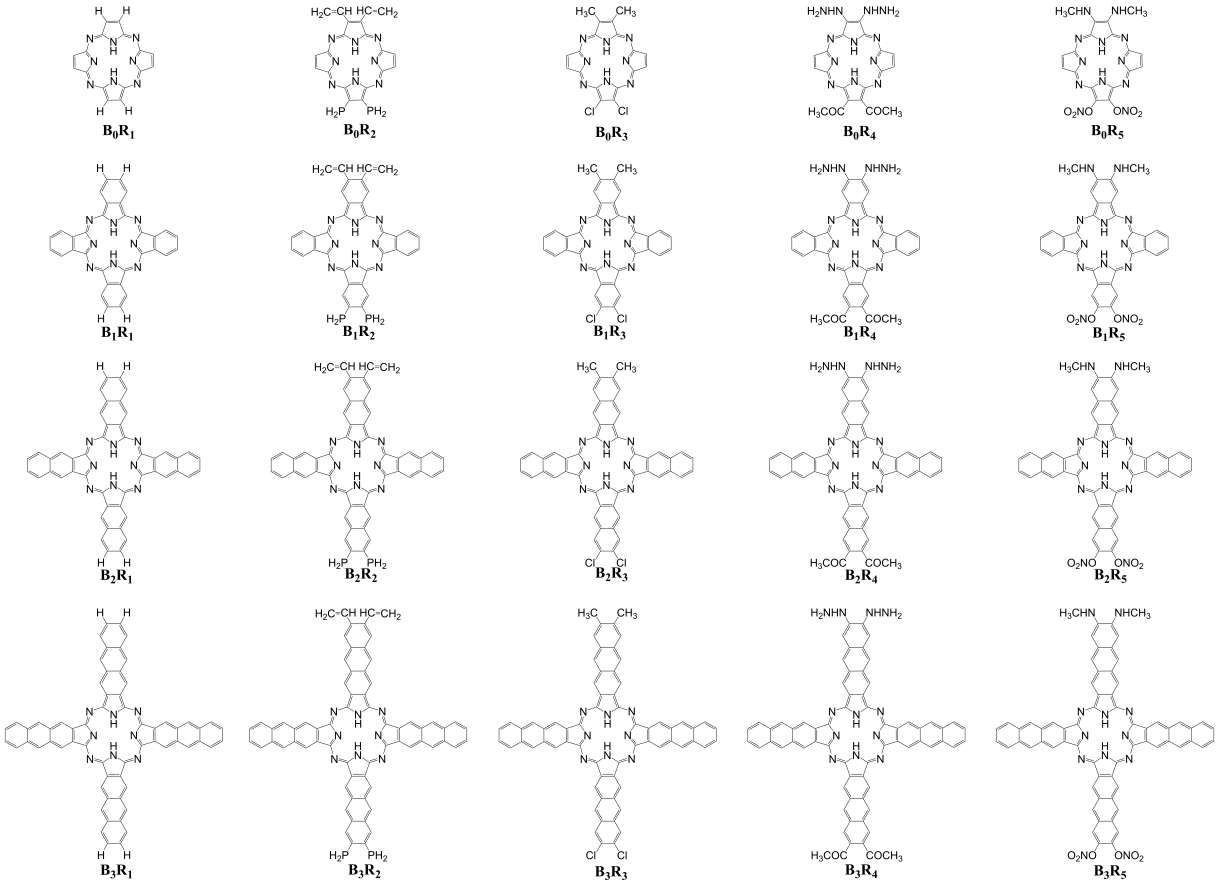

Scheme 1. Sketch and abbreviated names of Pc derivatives in this study.

2.1. Linear optical properties

We calculated the linear optical properties of a series of Pc derivatives. As shown in Figure 1, the UV-vis spectra can be divided into 3 areas according to different electron transition models.

The series of B_2R_n is chosen as the representative to investigate because of their high second-order nonlinear optical response coefficient, shown in the following part of this paper. The absorption band in Region I from 650 to 720 nm is mainly a result of the $\pi-\pi^*$ electron transitions of HOMO$\rightarrow$LUMO/LUMO+1, which is assigned to the Q bands (Figure 2). It is worth noting that along with the expansion of the conjugated system from B_0, B_1, B_2, to B_3, the Q bands are significantly red-shifted due to the decrease in the gap between HOMO and LUMO/LUMO+1. In addition, the absorption band of Region II from 270 to 370 nm mainly comes from the $\pi-\pi^*$ electron transitions from the core-level occupied orbitals to LUMO/LUMO+1. As can be seen in Figure 2, the corresponding electron densities transfer between the peripheral benzene and

the central Pc ring. This kind of electron transfer only occurs in the B_3R_n skeleton, which possesses enough fused benzene rings.

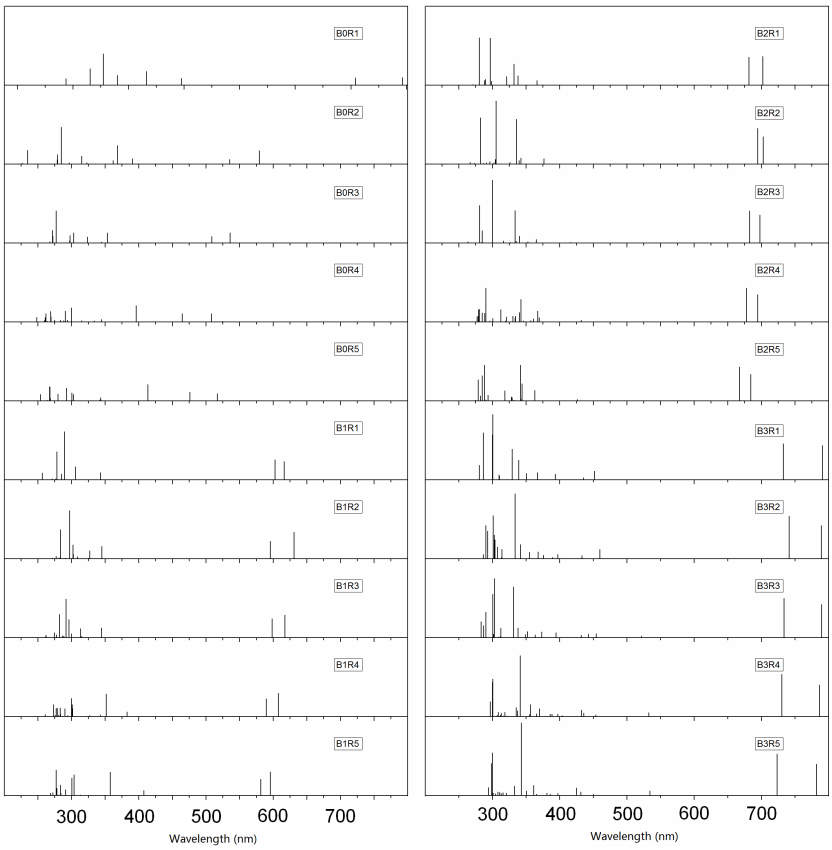

Figure 1. Simulated UV-vis spectrum of Pc derivatives.

2.2. Size effect

As shown in Figure 3, the β_{HRS} value of the analogues B_nR_5 increases with an increase in the peripherally conjugated systems, from 1365 a.u. for B_0R_5, 7655 a.u. for B_1R_5, to 10,496 a.u. for B_2R_5, revealing a moderate trend upward. However, it is worth noting that the β_{HRS} value decreases to 7478 a.u. for B_3R_5 along with a further increase in the peripherally conjugated skeleton, showing the limit when the expansion of conjugated system is selected to improve the hyper-Rayleigh scattering response coefficient.

According to previous research, the NLO response is to a large extent dependent on π electron delocalization and flowability. Therefore, expansion of π conjugated systems could increase the number of free π electrons and then enhance NLO response. When the conjugated part is large enough with ample free π electrons, the electron-transferring pathway will be too long to further improve the β value. In addition, excessive conjugation will also limit the electron oscillation because an increased external driven force provided by the external electronic field is required. Consequently, excessive conjugation will take disadvantage of enhancing the NLO response. Similar cases were also found in the investigation of subphthalocyanine.[17]

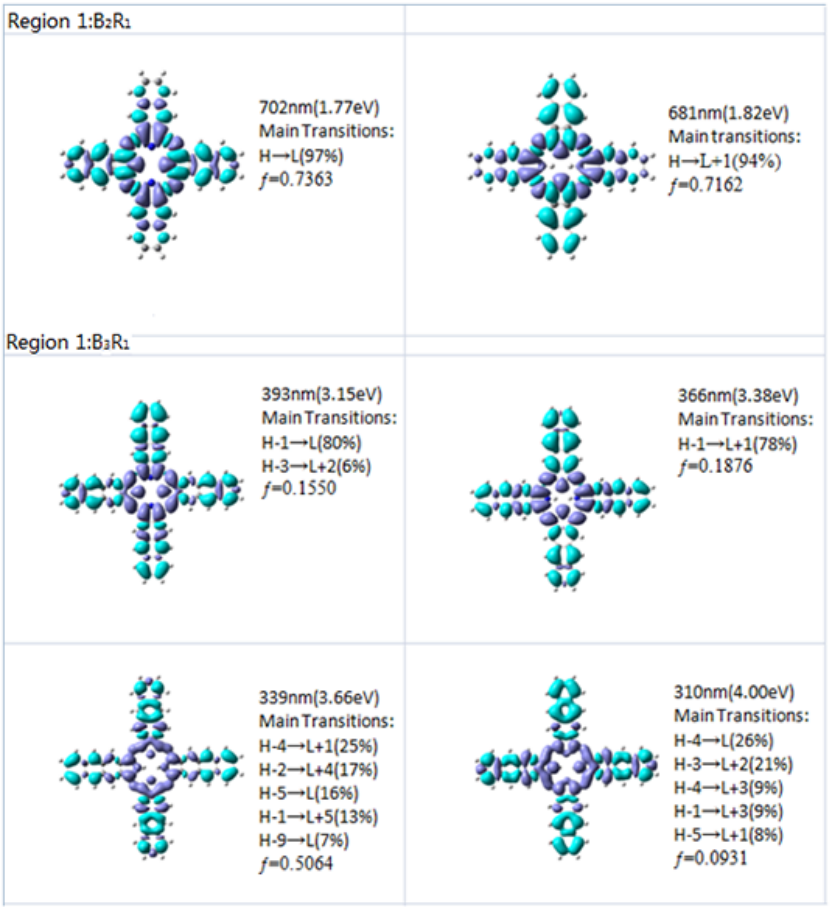

Figure 2. Electron densities transfer from the green areas to the blue ones. (Assignment: H = HOMO, L = LUMO, L+1 = LUMO+1, H-1 = HOMO-1, etc.).

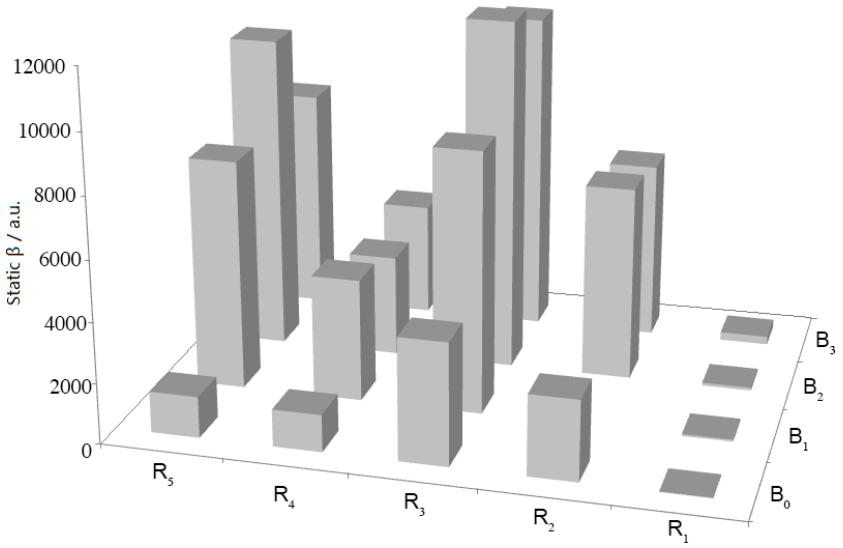

Figure 3. Static β_{HRS} of Pc derivatives.

2.3. Substitute effect

According to the calculation results, the β_{HRS} value first increases from 270 a.u. for B_3R_1, 5958 a.u. for B_3R_2, to 10747 a.u for B_3R_3, showing the direct relationship between the electronegativity of the peripheral push–pull substitutes and the second-order NLO response coefficient. This relationship is in agreement with the normal viewpoint. Nevertheless, for B_3R_4 and B_3R_5, the β_{HRS} decreases to 3809 a.u. for B_3R_4 and 7478 a.u. for B_3R_5. It is worth noting that the electronegativity difference between R_4 and R_5 is indeed stronger than that between R_1 and R_3. However, the geometries of –NHMe and $–ONO_2$ are too special to construct a pure dipolar moment, yet leading to an electrostatic potential system with a strong octupolar moment. To visualize this octupolar moment, the electrostatic potentials (EPs) of the whole series of B_nR_5 (n = 0, 1, 2, 3) were also calculated (Scheme 2). When –NHMe/$–ONO_2$ are introduced onto the periphery of the phthalocyanine ring in an unsymmetrical manner, the EPs are also asymmetrically distributed in the space near the molecule. As can be seen, the negative polarization (red) and the positive polarization (yellow) are alternately arranged, where the negative polarization area is close to the groups of $–ONO_2$ and the central conjugated ring; meanwhile, the positive polarization area is nearly spread all over the isoindole fragments and the groups of –NHMe. In summary, a (–)–(3+)–(3–)–(+) distribution is formed from this unusual population, which is a $C_{\infty v}$-type of octupolar moment.

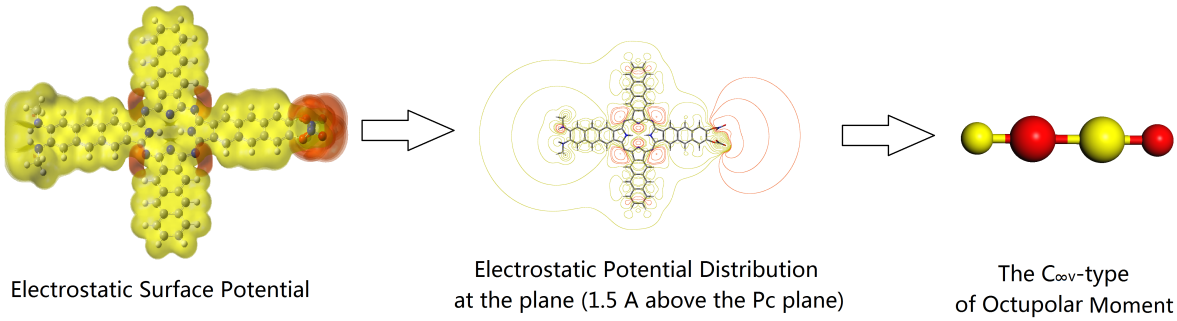

Scheme 2. Electrostatic potential population and octupolar moment simulation model of B_3R_5.

To further explore the evolution of dipolar/octupolar of these Pc derivatives, a polarization scan of HRS intensity was also carried out. For all the Pc derivatives, the normalized HRS intensity ($I_{\Psi V}^{2\omega}$) can be considered a function of the polarization angle (Ψ) of the incident light (Eq. (3)). The ($I_{\Psi V}^{2\omega}$)–Ψ schemes are listed in Figure 4. Along with the electronegativity and conjugated skeletons change, an apparent evolution of dipolar/octupolar occurred from B_3R_1 to B_3R_4. As can be seen, nearly half of these series of Pc derivatives can be considered dipolar molecules with the dipolar contribution $\Phi(\beta_{J=1}) \geq 50\%$, while the others possess more than 50% octupolar contribution.

2.4. Dynamic hyperpolarizability: dispersion effect

In order to explore the effect of frequency dispersion, the dynamic perturbations were also calculated at the same level. Four fundamental optical wavelengths with $\lambda = 1907$, 1460, 1340, and 1064 nm used in NLO measurements were employed to research the dispersion correction contribution to the NLO response using Eq. (7) (shown below). All the dynamic β_{HRS} value of each molecule versus its static β_{HRS} value is shown in Figure 5. As can be seen, the ratio of dynamic β_{HRS} values is about 1:1.192:1.542:1.620:1.716 for β_{HRS}(static):β_{HRS}(1907

nm):β_{HRS}(1460 nm):β_{HRS}(1340 nm):β_{HRS}(1064 nm), indicating that the dynamic β_{HRS} value increases along with the energy of incident light.

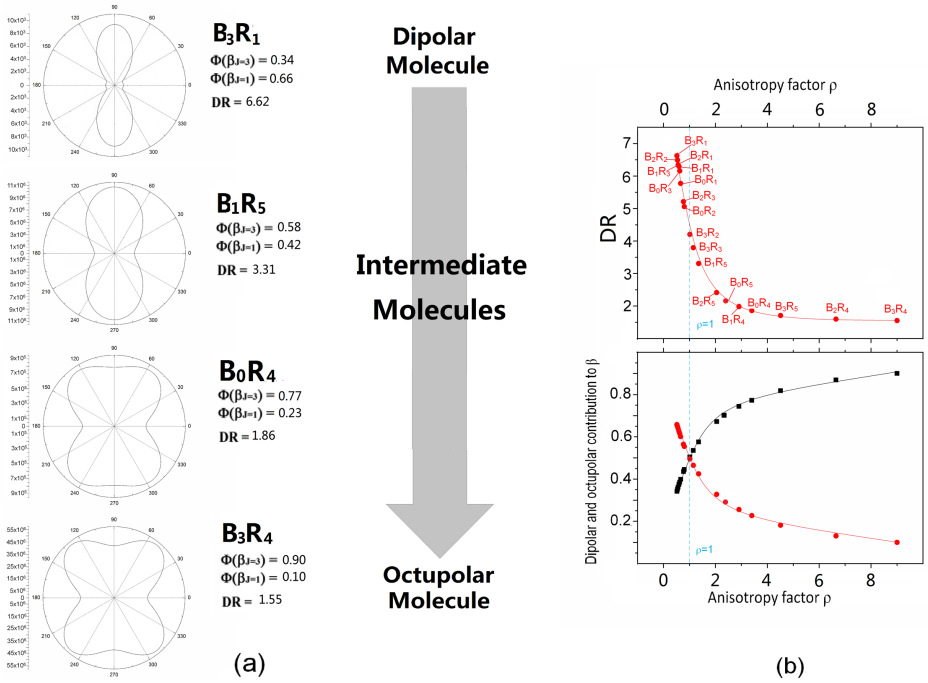

Figure 4. (a) Harmonic light intensity as a function of the polarization angle Ψ by polar representation. (b) Evolution of depolarization ratio DR as well as the octupolar $[\Phi(\beta_{J=3})]$ and dipolar $[\Phi(\beta_{J=1})]$ contributions to the second-order NLO response as a function of anisotropy factor.

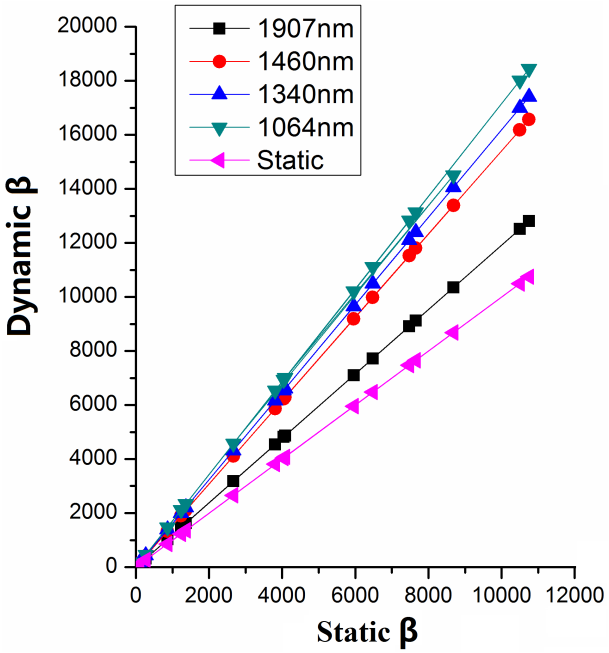

Figure 5. Dynamic hyperpolarizabilities of the full series of Pc derivatives versus its static value at 1907, 1460, 1340, and 1064 nm.

In order to further explore the nature of the second-order NLO effects, we simulated the behavior of the molecule driven by the external electromagnetic field, which could visually provide the details of electron density flowing paths.

As shown in Figure 6, the electron density appears as a complete oscillation. When the value of the electric field is periodically changing, the electronic density is also forced to transfer from one side to another side of the molecule, revealing the excellent mobility of the free π conjugated electrons. When the energy of incident light increases, the driving force on the free π electrons also increases, which is related to the fact that the dynamic β_{HRS} value at the high incident light energy is larger than that at the low incident light energy.

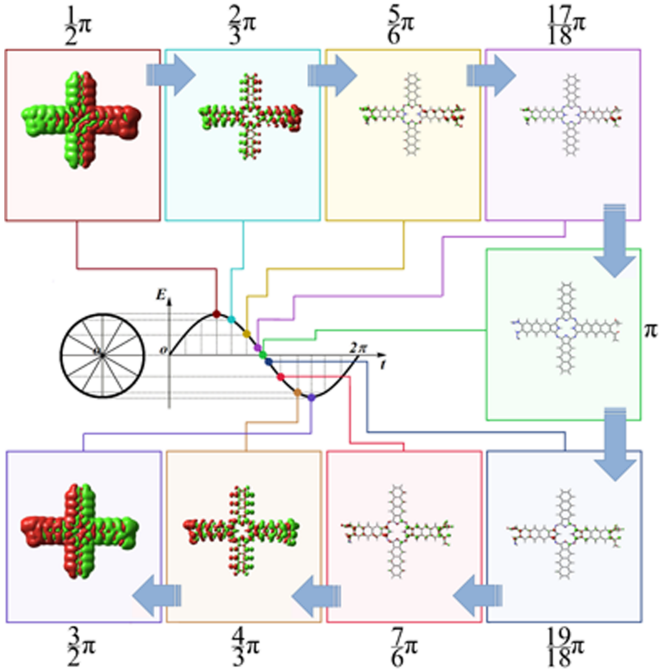

Figure 6. The periodical vibration of electric distribution driven by the external electromagnetic field with the electric field direction along the xy plane (Pc plane) employed. Electron density moves from the green area to the red area.

In conclusion, based on the density functional theory, the hyper-Rayleigh scattering response coefficients of a series of phthalocyanine derivatives were calculated, discovering the limitation when the expansion of the conjugated system is employed to improve the hyper-Rayleigh scattering response coefficient. Furthermore, an unusually $C_{\infty v}$-type octupolar population was found by potential analysis, showing the octupolar contribution to the second-order nonlinear optical responses in these functional phthalocyanine materials. In addition, both the dynamic and static hyper-Rayleigh scattering responses (β_{HRS}) were simulated using the coupled perturbed density functional theory, showing an increasing dynamic β_{HRS} value along with an increase in incident light energy.

3. Experimental

3.1. General theory about second-order nonlinear optical responses

Champagne and co-workers developed an effective method to evaluate the hyper-Rayleigh scattering (HRS) response $\beta_{HRS}(-2\omega;\ \omega,\ \omega)$,[18–20] which is described as

$$\beta_{HRS}(-2\omega;\omega,\omega) = \sqrt{\langle\beta^2_{ZZZ}\rangle + \langle\beta^2_{XZZ}\rangle} \tag{1}$$

where $\langle\beta^2_{ZZZ}\rangle$ and $\langle\beta^2_{XZZ}\rangle$ are the orientational average of the molecular tensor components, which can be calculated using the following equations:

$$\langle\beta^2_{ZZZ}\rangle = \frac{1}{7}\sum_{\zeta}^{z,y,z}\beta^2_{\zeta\zeta\zeta} + \frac{9}{35}\sum_{\zeta=\eta}^{z,y,z}\beta^2_{\eta\zeta\zeta} + \frac{2}{35}\sum_{\zeta\neq\eta\neq\xi}^{z,y,z}\beta^2_{\zeta\eta\xi} + \frac{6}{35}\sum_{\zeta\neq\eta}^{z,y,z}\beta_{\zeta\zeta\zeta}\beta_{\zeta\eta\eta} + \frac{3}{35}\sum_{\zeta\neq\eta\neq\xi}^{z,y,z}\beta_{\eta\zeta\zeta}\beta_{\eta\xi\xi} \tag{2a}$$

$$\langle\beta^2_{ZXX}\rangle = \frac{1}{35}\sum_{\zeta}^{z,y,z}\beta^2_{\zeta\zeta\zeta} + \frac{11}{105}\sum_{\zeta=\eta}^{z,y,z}\beta^2_{\eta\zeta\zeta} + \frac{4}{105}\sum_{\zeta\neq\eta\neq\xi}^{z,y,z}\beta^2_{\zeta\eta\xi} + \frac{2}{105}\sum_{\zeta\neq\eta}^{z,y,z}\beta_{\zeta\zeta\zeta}\beta_{\zeta\eta\eta} + \frac{1}{105}\sum_{\zeta\neq\eta\neq\xi}^{z,y,z}\beta_{\eta\zeta\zeta}\beta_{\eta\xi\xi} \tag{2b}$$

Furthermore, the molecular geometric information is given by the depolarization ratio (DR), which is expressed by $DR = \frac{\langle\beta^2_{ZZZ}\rangle}{\langle\beta^2_{ZXX}\rangle}$.

To further investigate the nature of the symmetric Rank-3 β tensor, $<\beta HRS^2>$ can be decomposed as the sum of the dipolar ($\beta J = 1$) and octupolar ($\beta J = 3$) tensorial components, which are shown as

$$\beta_{HRS} = \sqrt{(\beta^2_{HRS})} = \sqrt{\frac{10}{45}\left|\beta_{J=1}\right|^2 + \frac{10}{105}\left|\beta_{J=3}\right|^2} \tag{3}$$

$$\left|\beta_{J=1}\right|^2 = \frac{3}{5}\sum_{\xi}^{x,y,z}\beta^2_{\xi\xi\xi} + \frac{6}{5}\sum_{\xi\neq\eta}^{x,y,z}\beta_{\xi\xi\xi}\beta_{\xi\eta\eta} + \frac{3}{5}\sum_{\xi\neq\eta}^{x,y,z}\beta^2_{\eta\xi\xi} + \frac{3}{5}\sum_{\zeta\neq\eta\neq\xi}^{x,y,z}\beta_{\eta\xi\xi}\beta_{\eta\zeta\zeta} \tag{4a}$$

$$\left|\beta_{J=3}\right|^2 = \frac{2}{5}\sum_{\xi}^{x,y,z}\beta^2_{\xi\xi\xi} - \frac{6}{5}\sum_{\xi\neq\eta}^{x,y,z}\beta_{\xi\xi\xi}\beta_{\xi\eta\eta} + \frac{12}{5}\sum_{\xi\neq\eta}^{x,y,z}\beta^2_{\eta\xi\xi} - \frac{3}{5}\sum_{\zeta\neq\eta\neq\xi}^{x,y,z}\beta_{\eta\xi\xi}\beta_{\eta\zeta\zeta} + \sum_{\zeta\neq\eta\neq\xi}^{x,y,z}\beta^2_{\xi\eta\zeta} \tag{4b}$$

The nonlinear anisotropy parameter $\rho = \left|\beta_{J=3}\right| / \left|\beta_{J=1}\right|$ is defined to evaluate the ratio of the octupolar $[\Phi_{J=3} = \rho/(1+\rho)]$ and dipolar $[\Phi_{J=1} = 1/(1+\rho)]$ contribution to the hyperpolarizability tensor.

Moreover, assuming a general elliptically polarized incident light propagating along the X direction, the intensity of the harmonic light scattered at 90° along the Y direction and vertically polarized along the Z axis are given by Bersohn's expression:

$$I^{2\omega}_{\Psi V} \propto \left\langle\beta^2_{ZXX}\right\rangle\cos^4\Psi + \left\langle\beta^2_{ZZZ}\right\rangle\sin^4\Psi + \sin^2\Psi\cos^2\Psi \times \left\langle\left(\beta_{ZXZ} + \beta_{ZZX}\right)^2 - 2\beta_{ZZZ}\beta_{ZXX}\right\rangle \tag{5}$$

where the orientational average $\left\langle\left(\beta_{ZXZ} + \beta_{ZZX}\right)^2 - 2\beta_{ZZZ}\beta_{ZXX}\right\rangle$ is shown as

$$\begin{aligned}\left\langle\left(\beta_{ZXZ} + \beta_{ZZX}\right)^2 - 2\beta_{ZZZ}\beta_{ZXX}\right\rangle &= 7\left\langle\beta^2_{ZXX}\right\rangle - \left\langle\beta^2_{ZZZ}\right\rangle = \tfrac{2}{35}\sum_{\xi}^{x,y,z}\beta^2_{\xi\xi\xi} - \tfrac{32}{105}\sum_{\xi\neq\eta}^{x,y,z}\beta_{\xi\xi\xi}\beta_{\xi\eta\eta} \\ &\quad + \tfrac{10}{21}\sum_{\xi\neq\eta}^{x,y,z}\beta^2_{\eta\xi\xi} - \tfrac{16}{105}\sum_{\xi\neq\eta\neq\zeta}^{x,y,z}\beta_{\eta\xi\xi}\beta_{\eta\zeta\zeta} + \tfrac{22}{105}\sum_{\xi\neq\eta\neq\zeta}^{x,y,z}\beta^2_{\xi\eta\zeta}\end{aligned} \tag{6}$$

However, the above formulae are valid only in the off-resonance region. In the resonance region, the damping parameter, λ, should be taken into consideration using the following equations:[20]

$$\beta = \beta_0\frac{\omega_0^2}{3}\int\frac{1}{\sqrt{\pi}G}\exp\left(-\frac{y^2}{G^2}\right)F(\omega_0 + y)dy \tag{7a}$$

$$F(\omega) = \frac{1}{(\omega_0 + i\lambda + 2\omega)(\omega_0 + i\lambda + \omega)} + \frac{1}{(\omega_0 - i\lambda - 2\omega)(\omega_0 - i\lambda - \omega)} + \frac{1}{(\omega_0 + i\lambda + \omega)(\omega_0 - i\lambda - \omega)} \quad (7b)$$

where β_0 stands for total second-order NLO response coefficient, ω_0 stands for top wave length at the absorption peak, G stands for Gaussian width, y stands for the length behind the peak, and ω stands for excitation wavelength.

3.2. Density functional theory calculations

As early as in 2000, Champagne and co-workers pointed out that the conventional DFT methods present serious drawbacks when evaluating the linear and nonlinear electric field responses of push–pull π-conjugated systems.[21] Fortunately, the range separated hybrid functional CAM-B3LYP, which combines the hybrid qualities of B3LYP and the long-range correction,[22] has been proposed specifically to overcome the limitations of the conventional density functional according to Yanai and therefore has become a good candidate for the evaluation of the NLO properties of molecular materials.[23–25] In addition, it has been proved that CAM-B3LYP significantly improves the agreement between the calculated and experimental structural results in comparison with the most popular functional B3LYP.

In the present study, DFT, TD-DFT, and CP-DFT[12–15] were employed to study the nonlinear optical property. The molecule structures with all real frequencies were optimized at the level of CAM-B3LYP/6-311G(2df). Based on the optimized structures, the static ($\lambda = \infty$) and dynamic (λ = 1064, 1340, 1460, and 1907 nm) second-order polarizabilities were calculated together with the dipolar/octupolar contributions and the harmonic light intensity as a function of the polarization angle by polar representation. All the calculations were carried out using Gaussian 09 D.01[26] and NLO Calculator 0.21.[27]

Acknowledgments

Financial support from the National Key Basic Research Program of China (Grant Nos. 2013CB933402 and 2012CB224801), Natural Science Foundation of China, Beijing Municipal Commission of Education, University of Science and Technology Beijing, China Postdoctoral Science Foundation, and Beijing Natural Science Foundation is gratefully acknowledged.

References

1. Ray, P. *Chem. Rev.* **2010**, *110*, 5332–5365.
2. Haque, S.; Nelson, J. *Science* **2010**, *327*, 1466–1467.
3. Lim, G.; Chen, J.; Clark, J.; Goh, R. G. S.; Ng, W.-H.; Tan, H.-W.; Friend, R. H.; Ho, P. K.; Chua, L.-K. *Nature Photonics* **2011**, *5*, 554–560.
4. Hales, J. M.; Matichak, J.; Barlow, S.; Ohira, S.; Yesudas, K.; Bredas, J. L.; Perry, J. W.; Marder, S. R. *Science* **2010**, *327*, 1485–1488.
5. Prasad, N.; Williams, J. *Introduction to Nonlinear Optical Effects in Molecules and Polymers;* John Wiley: New York, NY, USA, 1991.
6. Nikogosyan, N. *Nonlinear Optical Crystals: A Complete Survey.* Springer Science and Business Media, Inc.: New York, NY, USA, 2005.
7. Wang, C.; Zhang, T.; Lin, W. *Chem. Rev.* **2012**,*112,* 1084–1104.

8. Boyd, R. *Nonlinear Optics*; Academic Press, Elsevier, 2008.
9. Verbiest, T.; Calys, K.; Rodriguez, V. Second-Order Nonlinear Optical Characterization Techniques, CRC Press, Taylor & Francis Group. 2009.
10. Jiang, J. *Functional Phthalocyanine Molecular Materials*; Springer: Heidelberg, Germany, 2010.
11. Albert, L.; Marks, T. J.; Ratner, M. A. *J. Am. Chem. Soc.* **1997**, *119*, 6575–6582.
12. Casida, M.; Huix-Rotllant, M. *Annu. Rev. Phys. Chem.* **2012**, *63*, 287–323.
13. Leang, S.; Zahariev, F.; Gordon, M. S. *J. Chem. Phys.* **2012**, *136*, 104101.
14. Wang, Z.; Zhang, L.; Chen, X.; Cukier, R. I.; Bu, Y. *J. Phys. Chem. B.* **2009**, *113*, 8222–8226.
15. Wang, J.; Sun, L.; Bu, Y. *J. Phys. Chem. B* **2010**, *114*, 1144–1147.
16. Hansch, C.; Leo, A.; Taft, R. W. *Chem. Rev.* **1991**, *91*, 165–195.
17. Zhang, L.; Qi, D.; Zhao, L. *J. Phy. Chem. A.* **2012**, *116*, 10249-10256.
18. Castet, F.; Bogdan, E.; Plaquet, A.; Ducasse, L.; Champagne, B.; Rodriguez, V. *J. Chem. Phys.* **2012**, *136*, 024506.
19. Plaquet, A.; Guillaume, M.; Champagne, B.; Castet, F.; Ducasse, L.; Pozzo, L.; Rodriguez, V. *Phys. Chem. Chem. Phys.* **2008**, *10*, 6223–6232.
20. Berkovic, G.; Meshulam,G.; Kotler Z. *J. Chem. Phys.* **2000**, *112,* 3997–4003.
21. Champagne, B.; Perpete, E. A.; Jacquemin, D.; van Gisbergen, A.; Baerends, E.; Soubra-Ghaoui, C.; Robins, A.; Kirtman, B. *J. Phys. Chem. A.* **2000**, *104*, 4755–4763.
22. Tawada, Y.; Tsuneda, T.; Yanagisawa, S.; Yanai, T.; Hirao, K. *J. Chem. Phys.* **2004**, *120*, 8425–8433.
23. Hu, Y.; Sun, S.; Zhong, R.; Xu, H.; Su, Z. *J. Phys. Chem. C.* **2011**, *115*, 18545–18551.
24. Zhang, C.; Xu, H.; Hu, Y.; Sun, S.; Su, Z. *J. Phys. Chem. A.* **2011**, *115*, 2035–2040.
25. Liu, C.; Guan, X.; Su, Z. *J. Phys. Chem. C.* **2011**, *115*, 6024–6032.
26. Frisch, M. J.; Trucks, G. W.; Schlegel, H. B.; Scuseria, G. E.; Robb, M. A.; Cheeseman, J. R.; Scalmani, G.; Barone, V.; Mennucci, B.; Petersson, G. A.; et al. Gaussian 09 (Version A.02); Gaussian, Inc.: Wallingford, CT, USA, 2009.
27. Qi, D.; Jiang J. *NLO Calculator (Version 0.21)*; University of Science and Technology Beijing: Beijing, China, 2013.